iScience

CellPress
OPEN ACCESS

Article

Structural basis of copper-efflux-regulator-dependent transcription activation

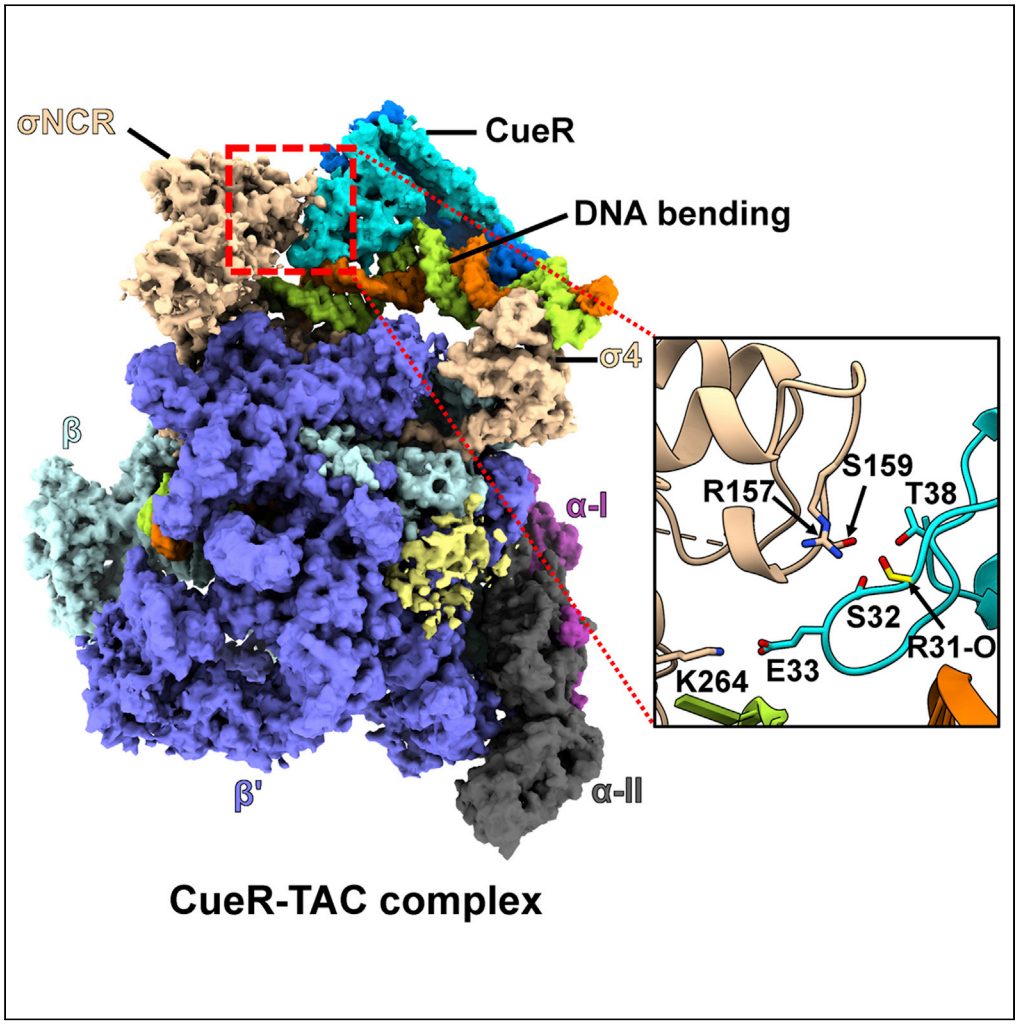

Wei Shi, Baoyue Zhang, Yanan Jiang, ..., Yang Yang, Yangbo Hu, Bin Liu

yan9yang@iastate.edu (Y.Y.)
ybhu@wh.iov.cn (Y.H.)
liu00794@umn.edu (B.L.)

Highlights

Cryo-EM structures of intact CueR-TAC complex without and with RNA synthesis

CueR dimer activates transcription through bending promoter DNA

The structures reveal the interactions between σNCR and CueR

The σNCR/CueR interactions play an auxiliary role in CueR-dependent transcription

Shi et al., iScience 24, 102449
May 21, 2021
https://doi.org/10.1016/j.isci.2021.102449

iScience

CellPress
OPEN ACCESS

Article

Structural basis of copper-efflux-regulator-dependent transcription activation

Wei Shi,[1,9] Baoyue Zhang,[2,3,9] Yanan Jiang,[1,4,9] Chang Liu,[5,9] Wei Zhou,[2,3] Ming Chen,[2,3] Yang Yang,[6,7,8,*] Yangbo Hu,[2,*] and Bin Liu[1,10,*]

SUMMARY

The copper efflux regulator (CueR), a representative member of mercury resistance regulator (MerR) family metalloregulators, controls expression of copper homeostasis-regulating genes in bacteria. The mechanism of transcription activation by CueR and other MerR family regulators is bending the spacer domain of promoter DNA. Here, we report the cryo-EM structures of the intact CueR-dependent transcription activation complexes. The structures show that CueR dimer bends the 19-bp promoter spacer to realign the −35 and −10 elements for recognition by σ^{70}-RNA polymerase holoenzyme and reveal a previously unreported interaction between the DNA-binding domain (DBD) from one CueR subunit and the σ^{70} nonconserved region (σNCR). Functional studies have shown that the CueR-σNCR interaction plays an auxiliary role in CueR-dependent transcription, assisting the activation mechanism of bending promoter DNA by CueR dimer. Because DBDs are highly conserved in sequence and structure, this transcription-activating mechanism could be generally used by MerR family regulators.

INTRODUCTION

Copper is an essential and precisely regulated trace element for biological function in all living organisms. However, it can be highly toxic at high concentrations, and thus, the maintenance of copper homeostasis is vital to the survival of cells (Baksh and Zamble, 2019; Finney and O'Halloran, 2003; Lutsenko, 2010; Robinson and Winge, 2010; Waldron et al., 2009). As a member of the mercury resistance regulator (MerR) family regulators, which respond to environmental stimuli, such as metal-ion overload, oxidative stress, or xenobiotics (Brown et al., 2003), the copper efflux regulator (CueR) is sensitive to +1 transition-metal ions including Cu^+, Ag^+, and Au^+ ions (Brown et al., 2003; Changela et al., 2003; Stoyanov and Brown, 2003). Other metal-responsive metalloregulators in the family include MerR, HmrR, PmtR, ZntR, CadR, PbrR, SctR, and CoaR, all of which contribute to homeostasis of heavy metal ions in bacteria via regulating the transcription of heavy-metal-resistance genes (Brown et al., 2003). CueR controls the transcription of two copper-homeostasis genes, *copA* encoding a Cu^+-transporting P-type ATPase pump and *cueO* encoding a copper oxidase for detoxification (Outten et al., 2000; Petersen and Moller, 2000; Stoyanov et al., 2001; Yamamoto and Ishihama, 2005). Because CueR shows an extremely high affinity ($K_d = 2 \times 10^{-21}$ M) to Cu^+, it is often found in the activator form (Changela et al., 2003; Philips et al., 2015). Like many other MerR family regulators (Bachas et al., 2011; Heldwein and Brennan, 2001; Newberry et al., 2008; Watanabe et al., 2008), CueR acts on the DNA promoter with a 19-bp spacer, which exceeds the 17-bp optimal length for recognition by σ^{70} factor (Brown et al., 2003; Philips et al., 2015; Typas and Hengge, 2006).

Previous structural studies of CueR have explained its metal-ion selectivity and revealed the general activation mode by modulating local DNA conformations within the promoters (Changela et al., 2003; Joshi et al., 2012; Philips et al., 2015; Sameach et al., 2017). However, the complete mechanism of transcription activation, such as whether and how the regulators directly interact with RNA polymerase (RNAP), necessitates the structure of the transcription activation complex (TAC) of RNA polymerase with MerR family regulators.

In this study, we reported the structures of the intact CueR-dependent TAC (hereinafter referred to as CueR-TAC). In addition to elucidating the role of CueR in modulating promoter DNA in TAC, the structures also reveal a previously unreported interaction between CueR and σ^{70}, the auxiliary role of which is further corroborated by *in vitro* and *in vivo* functional assays. This transcription-activating mechanism could be generally used by other members in the MerR family.

[1]Section of Transcription & Gene Regulation, The Hormel Institute, University of Minnesota, Austin, MN, USA

[2]State Key Laboratory of Virology, Wuhan Institute of Virology, Center for Biosafety Mega-Science, Chinese Academy of Sciences, Wuhan, China

[3]University of Chinese Academy of Sciences, Beijing, China

[4]Department of Pathophysiology, School of Basic Medical Sciences, Zhengzhou University, Zhengzhou, China

[5]Department of Immunobiology, Yale School of Medicine, New Haven, CT, USA

[6]Roy J. Carver Department of Biochemistry, Biophysics and Molecular Biology, Iowa State University, Ames, IA, USA

[7]Department of Molecular, Cellular and Developmental Biology, Yale University, New Haven, CT, USA

[8]Howard Hughes Medical Institute, Yale University, New Haven, CT, USA

[9]These authors contributed equally

[10]Lead contact

*Correspondence: yan9yang@iastate.edu (Y.Y.), ybhu@wh.iov.cn (Y.H.), liu00794@umn.edu (B.L.)

https://doi.org/10.1016/j.isci.2021.102449

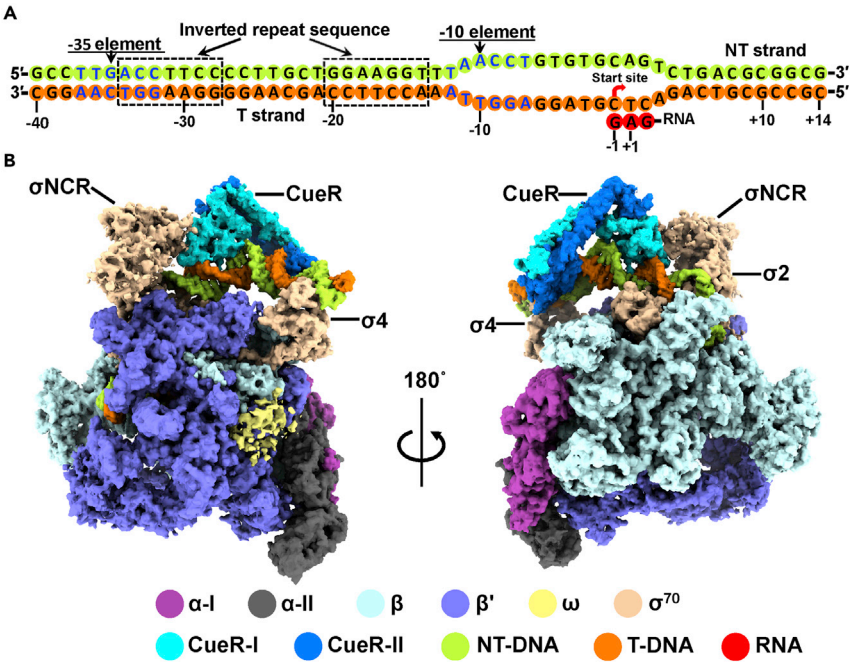

Figure 1. Overall structure of *E. coli* CueR-TAC with RNA transcript

(A) Schematic representation of the promoter DNA scaffold and the synthesized RNA in the cryo-EM structure of CueR-TAC with RNA transcript. The −35 and −10 elements (blue letters), inverted repeat sequence (dashed boxes), transcription bubble, transcription start site are indicated.

(B) Overviews of the cryo-EM map of *E. coli* CueR-TAC with RNA transcript. The individually colored density maps are displayed with two views in surface representation to indicate all the components of the complex. The same subunit color code is used throughout all figures.

See also Figures S1–S5, and Tables S1 and S2.

RESULTS AND DISCUSSION

Overall structures of CueR-TACs

The cryo-EM structures of the intact *Escherichia coli* CueR-TAC comprising a CueR dimer, σ^{70}-RNAP holoenzyme, and a complete CueR-specific promoter (P_{copA}) without or with a *de novo* synthesized RNA transcript were determined at overall resolutions of 3.9 Å and 4.1 Å, respectively (Figures S1–S3, Table S1). The CueR-TACs were reconstituted on a synthetic DNA scaffold that corresponds to positions −40 to +14 of P_{copA} and contains the −35 element, −10 element, and the inverted repeat sequence (IRS) for CueR binding (Figure 1A). The cryo-EM maps show well-defined density for all major components of the complexes and support reliable model building (Figures 1B, S4, and S5A). The two CueR-TAC structures are readily superimposable with an RMSD of 0.52 Å over their Cα atoms (Figure S5B), indicating that transitioning from open complex to initial transcribing complex does not require further conformational changes in CueR or promoter spacer DNA. The following structural analyses will focus on the CueR-TAC containing a *de novo* synthesized RNA transcript.

Promoter DNA modulation by CueR in TAC

In the complex, the CueR dimer sits on the top of the promoter spacer region with two N-terminal DNA-binding domains (DBDs) "gripping" the DNA backbone of the IRS like a clamp (Figure 2A). Although the IRS recognized by CueR has 3 bp overlap with the −35 element, CueR and RNAP holoenzyme bind to the opposite faces of spacer DNA to avoid possible steric clashes or interference with the −10 and −35 elements recognition (Figures 1B and 2A). The conformations of CueR dimer and its bound DNA in CueR-TAC are highly similar to those in the activator CueR/DNA complex (Figure 2A) (Philips et al., 2015), except that the bending of promoter spacer DNA in CueR-TAC is slightly reduced by ~3° compared with that in the activator CueR/DNA complex (Figure 2B), possibly owing to the insertion of σ4 helix-turn-helix (HTH) motif into the major groove from the opposite side. Using the canonical promoter with a 17-bp

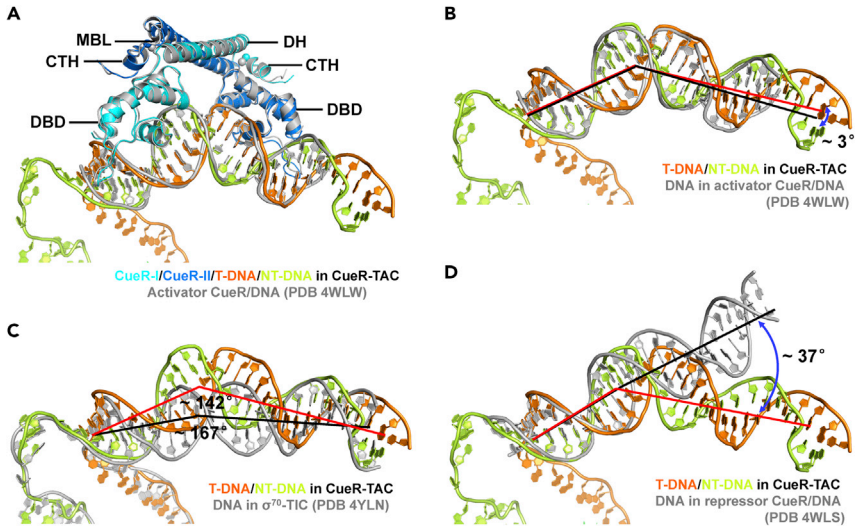

Figure 2. Comparisons of promoter DNA conformation among CueR-TAC, σ^{70}-TIC, repressor and activator CueR/DNA complexes

(A and B) Comparison of DNA conformation between CueR-TAC and activator CueR/DNA complex (PDB 4WLW). The activator CueR/DNA complex is colored in gray. The red and black lines are used to denote the helical axis of DNA. The angles formed between different sets of DNA axes are indicated. The two structures are superimposed by the downstream half of the DNA. DBD: DNA-binding domain; CTH: C-terminal α helix; DH: dimerization helix; MBL: metal-binding loop.

(C) Comparison of promoter DNA conformation between CueR-TAC and σ^{70}-TIC (PDB 4YLN). The promoter of σ^{70}-TIC is colored in gray.

(D) Comparison of DNA conformation between CueR-TAC and repressor CueR/DNA complex (PDB 4WLS). The DNA of repressor CueR/DNA complex is colored in gray. See also Figure S6.

spacer in the σ^{70}-transcription initiation complex (σ^{70}-TIC, PDB 4YLN) as a reference (Zuo and Steitz, 2015), the trajectory of the helical axis is altered by ~25° for the promoter spacer DNA in CueR-TAC (Figure 2C). In comparison with the repressor CueR/DNA complex structure in which the Cu^{+}-binding sites of CueR were deleted (Philips et al., 2015), the spacer DNA in CueR-TAC undergoes a significant directional change of ~37° (Figure 2D).

Like many other MerR family metalloregulators, CueR acts on the promoter with a 19-bp spacer, which is 2 bp longer than the optimal spacer length of 17 bp in σ^{70}-TIC. The additional 2 bp extends the distance between the −10 and −35 elements and hampers the proper recognition of −35 or −10 element, once one of the elements is fixed by σ^{70}-holoenzyme. The CueR dimer significantly bends DNA promoter, reducing the distance between the −35 and −10 elements to 55.4 Å, which is close to the 55.0 Å distance in the canonical promoter of σ^{70}-TIC (Figure S6). In addition, as observed in the activator CueR-DNA complex structure (Philips et al., 2015), this bending also under-twists the promoter, compensating for the phase angle change between the −35 and −10 elements caused by the extra 2 bp in the promoter spacer region. As a result, the −35 and −10 elements are properly recognized by σ^{70} in CueR-TAC as they are in σ^{70}-TIC (Figures S6B and S6C). *In vitro* promoter binding assays showed that P_{copA} was poorly bound by σ^{70}-RNAP holoenzyme in the absence of CueR protein and addition of CueR significantly increased the interaction between P_{copA} and σ^{70}-RNAP holoenzyme (Figures S6D and S6E).

CueR-σNCR interaction plays an auxiliary role on transcription activation

In addition to CueR-DNA interaction, CueR also makes protein-protein interaction with σ^{70} (Figure 3A). The DBDs of both CueR subunits interact with promoter spacer DNA by inserting the characteristic HTH motifs into DNA major grooves (Figures 3A and 3B), whereas only the DBD of CueR-I subunit makes contact with the σ^{70} nonconserved region (σNCR). The loop wing of CueR-I DBD interacts with the A153-S159 loop (loop L1) between σNCR helices H2 and H3, likely through the hydrogen bond interactions between S159 in σNCR and S32/T38 in CueR-I and between σNCR R157 and main chain oxygen atom of R31 in CueR-I, as well as a possible salt bridge interaction between σNCR K264 and CueR-I E33 (Figure 3C). Consistent

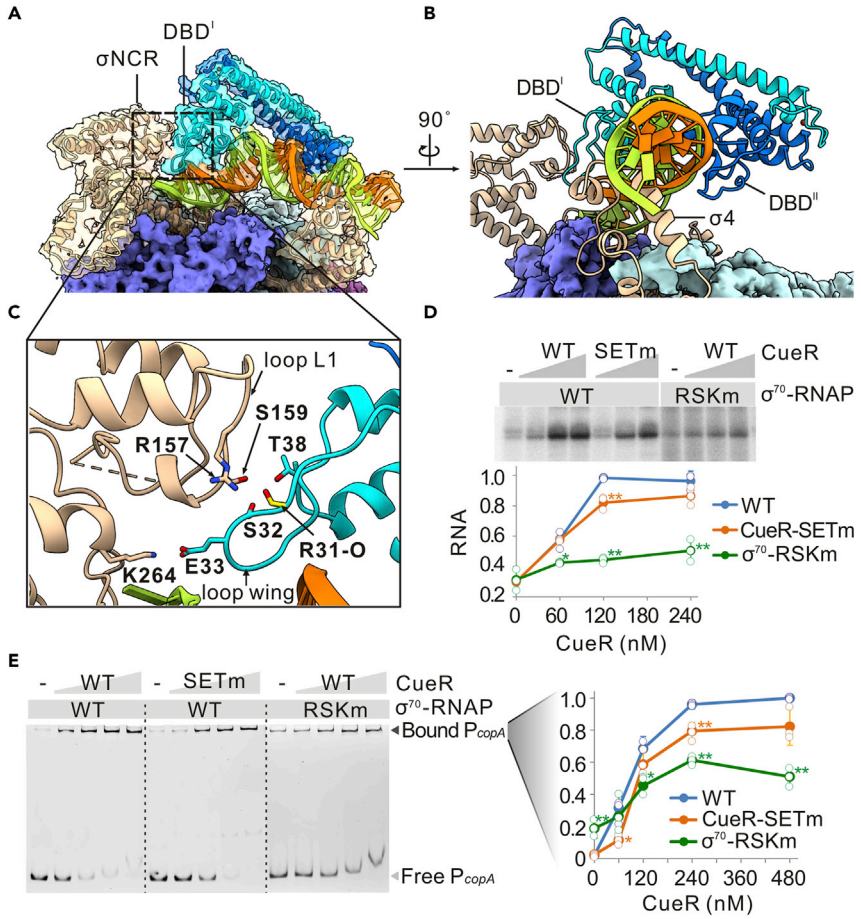

Figure 3. The influence of CueR-σNCR interaction on CueR-dependent transcription activation

(A) Overview of CueR-σNCR and CueR-promoter interactions in CueR-TAC. The cryo-EM densities for CueR, σ^{70}, and promoter DNA are shown in transparent surface representation using the combined map with clearer σNCR density.

(B) Side view of CueR dimer and neighboring regions in CueR-TAC.

(C) Close-up view of the dashed box area in (A), showing the detailed interaction between σNCR and CueR-I DBD.

(D) Roles of CueR-σNCR interaction in CueR-dependent transcription. *In vitro* transcription assays on double-stranded P_{copA} were performed using either wild-type CueR-RNAP-σ^{70} ternary complex or ternary complexes containing mutations on CueR (CueR-SETm: S32A/E33A/T38A) or σ^{70} (σ^{70}-RSKm: R157A/S159A/K264A). RNA products were quantified from three experiments and are shown as mean ± SD.

(E) Role of CueR-σNCR interaction in σ^{70}-RNAP-P_{copA} binding. Shifted P_{copA} bands from three experiments were quantified and are shown as mean ± SD in the right panel. *p < 0.05; **p < 0.01. See also Figures S7–S9 and Table S2.

with the aforementioned structural observations, mutations of S32, E33, and T38 of CueR to alanines (referred to as CueR-SETm) undermined the CueR's abilities in facilitating the binding of RNAP holoenzyme to P_{copA} and activating transcription on the promoter (Figures 3D, 3E, and S7A). Similarly, alanine substitutions of R157, S159, and K264 of σ^{70} (referred to as σ^{70}-RSKm) also decreased the transcription activation on P_{copA} by CueR (Figures 3D and S7A) and reduced the CueR-dependent enhancement of P_{copA} binding by RNAP holoenzyme, whereas the basal promoter binding activity of the σ^{70}-RSKm holoenzyme without CueR was not weakened (Figures 3E and S7B). Sequence alignments show that the residues involved in CueR-σNCR interactions are highly conserved (Figure S8). Therefore, the CueR-σNCR interaction plays an auxiliary role in CueR-dependent transcription, assisting the activation mechanism of bending promoter DNA by CueR dimer.

It should be noted that during the preparation of our manuscript, Fang et al also reported the cryo-EM structures of *E. coli* CueR transcription activation complex (Fang et al., 2020). All of their and our structures show that CueR activates transcription through bending the promoter DNA, supporting the DNA distortion

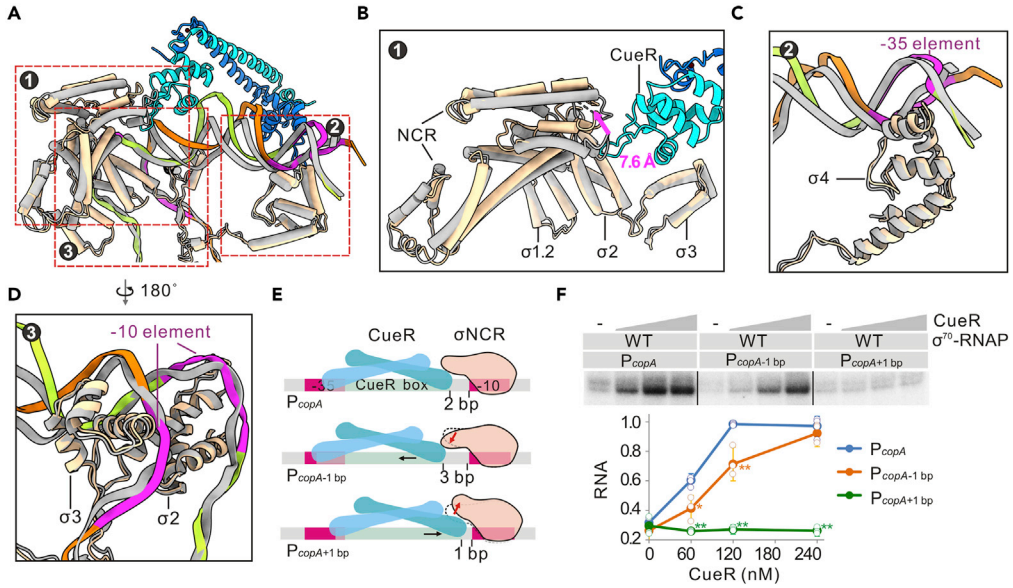

Figure 4. Roles of σNCR movement in CueR-activated transcription

(A) Structural comparisons of σ^{70} and promoters between CueR-TAC and σ^{70}-TIC (PDB 4YLN). −35 and −10 elements of CueR-TAC are colored in magenta. The structure of σ^{70}-TIC is colored in gray. The two structures are superimposed by σ2 and σ3 domains of σ^{70}.

(B) Close-up view of the boxed area 1 showing σNCR and CueR. The relative movement of loop L1 is marked by a magenta arrow and the distance of movement is indicated.

(C) Close-up view of −35 element and σ4 domain in the boxed area 2. The −35 element is colored in magenta.

(D) Close-up view of −10 element, σ2 and σ3 domains in the boxed area 3. The −10 element is colored in magenta.

(E) Schematic representation of P_{copA} mutations by moving the CueR box 1-bp closer to or away from the −10 element, which create promoters with 3 bp or 1 bp distances between CueR box and −10 element compared with the 2 bp distance in wild-type P_{copA}. Proposed movements of σNCR in CueR-dependent promoter recognition on mutated P_{copA} fragments compared with that on wild-type P_{copA} are indicated by red arrows.

(F) CueR-dependent activation of transcription on wild-type and mutated P_{copA} analyzed by *in vitro* transcription. RNA products were quantified from three independent tests and are shown as mean ± SD. *p < 0.05; **p < 0.01. See also Figure S10 and Table S2.

paradigm of allosteric transcriptional control. They found that mutation of residue E33 alone does not alter CueR activity, while simultaneous mutations of S32, E33, and T38 of CueR to alanines in our study slightly impaired CueR activity, indicating an auxiliary role of CueR-σNCR interaction in CueR-dependent transcription.

σNCR repositions upon CueR binding during transcription activation

The overall structures and promoter recognition patterns are highly similar between CueR-TAC and σ^{70}-TIC (PDB 4YLN) (Zuo and Steitz, 2015) (Figures 4A–4D and S6A-C), but the σNCR conformations are noticeably different in the two structures, likely owing to the CueR-σNCR interaction (Figures 4A and 4B). The loop wing of CueR-I DBD inserts into the gap between σNCR loop L1 and promoter DNA and pushes the loop L1 and two neighboring helices (H2 and H3) 7.6 Å away from their original positions (Figures 4B and S9A). Other σNCR helices also exhibit distance shifts to various extents (Figures 4B and S9A).

The residue R157 of σNCR has been suggested to interact with promoter template strand DNA at −16/−17 position. Disruption of the interaction by mutating the arginine to either alanine or glutamate impeded promoter DNA opening and greatly decreased transcription activity (Narayanan et al., 2018). In our CueR-TAC structure, R157 has established an interaction with CueR-I DBD instead (Figure 3C) and lost the proposed interaction with DNA. The DNA region that was contacted by σNCR in RNAP-σ^{70} open complex (PDB 6CA0) is now interacted by CueR-I DBD (Figures S9B and S9C). Therefore, in CueR-TAC, R157 adopts a role of stabilizing the CueR binding, while its original function in interacting with spacer DNA is substituted by the loop wing of CueR-I DBD, which is sandwiched between σNCR and spacer DNA (Figures 3C, S9B, and S9C).

The positional effects of IRS on CueR-σNCR interaction

To further understand the role of CueR-σNCR interaction in CueR-activated transcription, we designed two promoter mutants by moving the CueR core binding sequence (CCTTCC-N_7-GGAAGG) (Yamamoto and Ishihama, 2005) 1 bp upstream or downstream in the P_{copA} promoter (referred to as $P_{copA-1bp}$ and $P_{copA+1bp}$, respectively) in which the length of the spacer DNA was kept to be 19 bp as the wild-type P_{copA} (Figure S10A). For the two promoter mutants, the $P_{copA-1bp}$ is predicted to weaken the CueR-σNCR interaction in CueR-TAC complex owing to a longer distance between position of CueR-binding sequence and the −10 element (Figure 4E). By contrast, the $P_{copA+1bp}$ is predicted to cause a significant steric clash between CueR and σNCR owing to the closer position of CueR-binding sequence to the −10 element (Figure 4E). Both promoter mutants showed unaffected binding to CueR in the absence of RNAP (Figure S10B). However, the $P_{copA-1bp}$ caused a moderate decrease in CueR-dependent promoter binding by RNAP and activation of transcription, and both the CueR-dependent promoter binding and transcription activation were almost abolished on $P_{copA+1bp}$ (Figures 4F, S10C, and S10D). These data further indicate that CueR-σNCR interaction could stabilize the CueR-RNAP-promoter complex in activating transcription. In addition, the position of IRS on the P_{copA} is likely evolutionarily optimized for proper CueR-σNCR interaction and maximum activation of bacterial transcription by CueR.

Concluding remarks

Taken together, our data show that CueR bends the promoter DNA to facilitate the −10 and −35 elements recognition by RNAP and its interaction with σNCR stabilizes the CueR-RNAP-promoter complex. Our findings support that RNAP and CueR work synergistically in regulating transcription and increase each other's affinity to P_{copA} (Martell et al., 2015). This study advances the understanding of the transcription activation process regulated by bacterial metallosensor proteins and suggests that other MerR family factors likely also adopt a similar mode of action to bend promoter DNA and make contacts with σNCR domain during transcription activation, given that their N-terminal DNA-binding domains are highly conserved in the family (Brown et al., 2003; Philips et al., 2015).

Limitations of the study

In this study, we have captured the structures of CueR-TAC without RNA or with 3-nt RNA, showing the key activation states. However, the complete transcription activation process by CueR requires the elucidation of more states with RNA transcripts of different lengths.

STAR★METHODS

Detailed methods are provided in the online version of this paper and include the following:

- KEY RESOURCES TABLE
- RESOURCE AVAILABILITY
  - Lead contact
  - Material availability
  - Data and code availability
- EXPERIMENTAL MODEL AND SUBJECT DETAILS
- METHOD DETAILS
  - Purification of RNA polymerase core enzyme and preparation of σ^{70}-RNAP holoenzyme
  - Expression and purification of CueR
  - Assembly and purification of *E. coli* CueR-TAC complex
  - Cryo-EM sample preparation and data acquisition
  - Image processing
  - Model building and refinement
  - *In vitro* transcription assay
  - DNA-binding analysis
  - *E. coli* mutant construction
  - *In vivo* promoter activity test
- QUANTIFICATION AND STATISTICAL ANALYSIS

SUPPLEMENTAL INFORMATION

Supplemental information can be found online at https://doi.org/10.1016/j.isci.2021.102449.

ACKNOWLEDGMENTS

We thank the staff at the cryo-EM facility and instrument core facility in the Hormel Institute, University of Minnesota, which is funded by the Hormel Foundation, for providing help. We also thank the Core Facility and Technical Support of Wuhan Institute of Virology for help in radioactive and fluorescent tests. This work was supported by the starting-up funding from The Hormel Institute, University of Minnesota granted to B.L., the National Natural Science Foundation of China (31870133) and the Youth Innovation Promotion Association CAS (Y201750) to Y.H.

AUTHOR CONTRIBUTIONS

B.L. and Y.H. initiated and designed the experiments. W.S. and Y.J. performed protein sample preparations and assembly of the complexes used in the structure determination. W.S., Y.J. and B.L. performed cryo-EM grid preparation, screening, and optimization. B.L. conducted high throughput data collection on Titan Krios, Y.Y., C.L., W.S. and B.L. performed image processing, map reconstruction, and model building and refinement. B.Z., W.Z. and M.C. constructed mutations and purified proteins. B.Z., W.Z., M.C. and Y.H. performed *in vitro* biochemical and *in vivo* promoter activity tests. W.S., B.Z., Y.J., C.L., Y.Y., Y.H. and B.L. analyzed data. W.S., C.L., Y.Y., Y.H. and B.L. wrote the manuscript with the contributions from all the authors.

DECLARATION OF INTERESTS

The authors declare no competing interests.

Received: February 17, 2021
Revised: March 18, 2021
Accepted: April 14, 2021
Published: May 21, 2021

REFERENCES

Adams, P.D., Afonine, P.V., Bunkoczi, G., Chen, V.B., Davis, I.W., Echols, N., Headd, J.J., Hung, L.W., Kapral, G.J., Grosse-Kunstleve, R.W., et al. (2010). PHENIX: a comprehensive Python-based system for macromolecular structure solution. Acta Crystallogr. D Biol. Crystallogr. *66*, 213–221.

Afonine, P.V., Klaholz, B.P., Moriarty, N.W., Poon, B.K., Sobolev, O.V., Terwilliger, T.C., Adams, P.D., and Urzhumtsev, A. (2018). New tools for the analysis and validation of cryo-EM maps and atomic models. Acta Crystallogr. D Struct. Biol. *74*, 814–840.

Asarnow, D., Palovcak, E., and Cheng, Y. (2019). UCSF Pyem v0.5 (Zenodo).

Bachas, S., Eginton, C., Gunio, D., and Wade, H. (2011). Structural contributions to multidrug recognition in the multidrug resistance (MDR) gene regulator, BmrR. Proc. Natl. Acad. Sci. U S A *108*, 11046–11051.

Baksh, K.A., and Zamble, D.B. (2019). Allosteric control of metal-responsive transcriptional regulators in bacteria. J. Biol. Chem. *295*, 1673–1684.

Belogurov, G.A., Vassylyeva, M.N., Svetlov, V., Klyuyev, S., Grishin, N.V., Vassylyev, D.G., and Artsimovitch, I. (2007). Structural basis for converting a general transcription factor into an operon-specific virulence regulator. Mol. Cell *26*, 117–129.

Brown, N.L., Stoyanov, J.V., Kidd, S.P., and Hobman, J.L. (2003). The MerR family of transcriptional regulators. FEMS Microbiol. Rev. *27*, 145–163.

Changela, A., Chen, K., Xue, Y., Holschen, J., Outten, C.E., O'Halloran, T.V., and Mondragon, A. (2003). Molecular basis of metal-ion selectivity and zeptomolar sensitivity by CueR. Science *301*, 1383–1387.

Chen, V.B., Arendall, W.B., 3rd, Headd, J.J., Keedy, D.A., Immormino, R.M., Kapral, G.J., Murray, L.W., Richardson, J.S., and Richardson, D.C. (2010). MolProbity: all-atom structure validation for macromolecular crystallography. Acta Crystallogr. D Biol. Crystallogr. *66*, 12–21.

Emsley, P., and Cowtan, K. (2004). Coot: model-building tools for molecular graphics. Acta Crystallogr. D Biol. Crystallogr. *60*, 2126–2132.

Fang, C.L., Philips, S.J., Wu, X.X., Chen, K., Shi, J., Shen, L.Q., Xu, J.C., Feng, Y., O'Halloran, T.V., and Zhang, Y. (2020). CueR activates transcription through a DNA distortion mechanism. Nat. Chem. Biol. *17*, 57–64.

Finney, L.A., and O'Halloran, T.V. (2003). Transition metal speciation in the cell: insights from the chemistry of metal ion receptors. Science *300*, 931–936.

Goddard, T.D., Huang, C.C., Meng, E.C., Pettersen, E.F., Couch, G.S., Morris, J.H., and Ferrin, T.E. (2018). UCSF ChimeraX: Meeting modern challenges in visualization and analysis. Protein Sci. *27*, 14–25.

Heldwein, E.E., and Brennan, R.G. (2001). Crystal structure of the transcription activator BmrR bound to DNA and a drug. Nature *409*, 378–382.

Hu, Y., Lu, P., Wang, Y., Ding, L., Atkinson, S., and Chen, S. (2009). OmpR positively regulates urease expression to enhance acid survival of Yersinia pseudotuberculosis. Microbiology *155*, 2522–2531.

Hu, Y., Wang, Z., Feng, L., Chen, Z., Mao, C., Zhu, Y., and Chen, S. (2016). sigma(E) -dependent activation of RbpA controls transcription of the furA-katG operon in response to oxidative stress in mycobacteria. Mol. Microbiol. *102*, 107–120.

Jiang, Y., Chen, B., Duan, C., Sun, B., Yang, J., and Yang, S. (2015). Multigene editing in the Escherichia coli genome via the CRISPR-Cas9 system. Appl. Environ. Microbiol. *81*, 2506–2514.

Joshi, C.P., Panda, D., Martell, D.J., Andoy, N.M., Chen, T.Y., Gaballa, A., Helmann, J.D., and Chen, P. (2012). Direct substitution and assisted dissociation pathways for turning off transcription by a MerR-family metalloregulator. Proc. Natl. Acad. Sci. U S A *109*, 15121–15126.

Kucukelbir, A., Sigworth, F.J., and Tagare, H.D. (2014). Quantifying the local resolution of cryo-EM density maps. Nat. Methods *11*, 63–65.

Li, Y., Li, L., Huang, L., Francis, M.S., Hu, Y., and Chen, S. (2014). Yersinia Ysc-Yop type III secretion feedback inhibition is relieved through YscV-dependent recognition and secretion of LcrQ. Mol. Microbiol. *91*, 494–507.

Liu, B., Hong, C., Huang, R.K., Yu, Z., and Steitz, T.A. (2017). Structural basis of bacterial transcription activation. Science *358*, 947–951.

Lutsenko, S. (2010). Human copper homeostasis: a network of interconnected pathways. Curr. Opin. Chem. Biol. *14*, 211–217.

Martell, D.J., Joshi, C.P., Gaballa, A., Santiago, A.G., Chen, T.Y., Jung, W., Helmann, J.D., and Chen, P. (2015). Metalloregulator CueR biases RNA polymerase's kinetic sampling of dead-end or open complex to repress or activate transcription. Proc. Natl. Acad. Sci. U S A *112*, 13467–13472.

Narayanan, A., Vago, F.S., Li, K., Qayyum, M.Z., Yernool, D., Jiang, W., and Murakami, K.S. (2018). Cryo-EM structure of Escherichia coli sigma(70) RNA polymerase and promoter DNA complex revealed a role of sigma non-conserved region during the open complex formation. J. Biol. Chem. *293*, 7367–7375.

Newberry, K.J., Huffman, J.L., Miller, M.C., Vazquez-Laslop, N., Neyfakh, A.A., and Brennan, R.G. (2008). Structures of BmrR-drug complexes reveal a rigid multidrug binding pocket and transcription activation through tyrosine expulsion. J. Biol. Chem. *283*, 26795–26804.

Outten, F.W., Outten, C.E., Hale, J., and O'Halloran, T.V. (2000). Transcriptional activation of an Escherichia coli copper efflux regulon by the chromosomal MerR homologue, cueR. J. Biol. Chem. *275*, 31024–31029.

Petersen, C., and Moller, L.B. (2000). Control of copper homeostasis in Escherichia coli by a P-type ATPase, CopA, and a MerR-like transcriptional activator, CopR. Gene *261*, 289–298.

Pettersen, E.F., Goddard, T.D., Huang, C.C., Couch, G.S., Greenblatt, D.M., Meng, E.C., and Ferrin, T.E. (2004). UCSF Chimera–a visualization system for exploratory research and analysis. J. Comput. Chem. *25*, 1605–1612.

Philips, S.J., Canalizo-Hernandez, M., Yildirim, I., Schatz, G.C., Mondragon, A., and O'Halloran, T.V. (2015). Allosteric transcriptional regulation via changes in the overall topology of the core promoter. Science *349*, 877–881.

Punjani, A., Rubinstein, J.L., Fleet, D.J., and Brubaker, M.A. (2017). cryoSPARC: algorithms for rapid unsupervised cryo-EM structure determination. Nat. Methods *14*, 290–296.

Robert, X., and Gouet, P. (2014). Deciphering key features in protein structures with the new ENDscript server. Nucleic Acids Res. *42*, W320–W324.

Robinson, N.J., and Winge, D.R. (2010). Copper metallochaperones. Annu. Rev. Biochem. *79*, 537–562.

Rohou, A., and Grigorieff, N. (2015). CTFFIND4: Fast and accurate defocus estimation from electron micrographs. J. Struct. Biol. *192*, 216–221.

Rubinstein, J.L., and Brubaker, M.A. (2015). Alignment of cryo-EM movies of individual particles by optimization of image translations. J. Struct. Biol. *192*, 188–195.

Sameach, H., Narunsky, A., Azoulay-Ginsburg, S., Gevorkyan-Aiapetov, L., Zehavi, Y., Moskovitz, Y., Juven-Gershon, T., Ben-Tal, N., and Ruthstein, S. (2017). Structural and dynamics characterization of the MerR family metalloregulator CueR in its repression and activation states. Structure *25*, 988–996.e3.

Shi, W., Zhou, W., Zhang, B., Huang, S., Jiang, Y., Schammel, A., Hu, Y., and Liu, B. (2020). Structural basis of bacterial sigma(28) -mediated transcription reveals roles of the RNA polymerase zinc-binding domain. EMBO J. *39*, e104389.

Sievers, F., and Higgins, D.G. (2014). Clustal omega. Curr. Protoc. Bioinformatics *48*, 3 13 11–16.

Stoyanov, J.V., and Brown, N.L. (2003). The Escherichia coli copper-responsive copA promoter is activated by gold. J. Biol. Chem. *278*, 1407–1410.

Stoyanov, J.V., Hobman, J.L., and Brown, N.L. (2001). CueR (YbbI) of Escherichia coli is a MerR family regulator controlling expression of the copper exporter CopA. Mol. Microbiol. *39*, 502–511.

Tan, Y.Z., Baldwin, P.R., Davis, J.H., Williamson, J.R., Potter, C.S., Carragher, B., and Lyumkis, D. (2017). Addressing preferred specimen orientation in single-particle cryo-EM through tilting. Nat. Methods *14*, 793–796.

Typas, A., and Hengge, R. (2006). Role of the spacer between the -35 and -10 regions in sigmas promoter selectivity in Escherichia coli. Mol. Microbiol. *59*, 1037–1051.

Waldron, K.J., Rutherford, J.C., Ford, D., and Robinson, N.J. (2009). Metalloproteins and metal sensing. Nature *460*, 823–830.

Watanabe, S., Kita, A., Kobayashi, K., and Miki, K. (2008). Crystal structure of the [2Fe-2S] oxidative-stress sensor SoxR bound to DNA. Proc. Natl. Acad. Sci. U S A *105*, 4121–4126.

Yamamoto, K., and Ishihama, A. (2005). Transcriptional response of Escherichia coli to external copper. Mol. Microbiol. *56*, 215–227.

Zivanov, J., Nakane, T., and Scheres, S.H.W. (2020). Estimation of high-order aberrations and anisotropic magnification from cryo-EM data sets in RELION-3.1. IUCrJ *7*, 253–267.

Zuo, Y., and Steitz, T.A. (2015). Crystal structures of the E. coli transcription initiation complexes with a complete bubble. Mol. Cell *58*, 534–540.

STAR★METHODS

KEY RESOURCES TABLE

REAGENT or RESOURCE	SOURCE	IDENTIFIER
Bacterial and virus strains		
Ec-parent	Hu et al., 2016	N/A
Ec-CueR-SETm	This study	N/A
Ec-σ^{70}-RSKm	This study	N/A
E. coli BL21(DE3)	Novagen	Cat#69450-3
E. coli DH5α	Shenzhen KT Life	Cat#KTSM101L
Chemicals, peptides, and recombinant proteins		
rNTP	Promega	P1221
$CuSO_4$	SinoPharm	10008218
$AgNO_3$	Aladdin	S116264
[α-^{32}P]GTP	PerkinElmer	BLU006H500UC
Deposited data		
Combined cryo-EM map of CueR-TAC complex with clearer σNCR density	This study	EMD-22289
The atomic coordinates for the model of CueR-TAC complex without RNA transcript	This study	6XH7
The atomic coordinates for the model of CueR-TAC complex with RNA transcript	This study	6XH8
Cryo-EM map of CueR-TAC complex without RNA transcript	This study	EMD-22184
Cryo-EM map of CueR-TAC complex with RNA transcript	This study	EMD-22185
Oligonucleotides		
	See Table S2 for oligonucleotides and sequences.	
Recombinant DNA		
pET21a-σ^{70}-RSKm	This study	N/A
pET21a-CueR	This study	N/A
pET21a-CueR-SETm	This study	N/A
pCas	Jiang et al., 2015	N/A
pTargetF	Jiang et al., 2015	N/A
pTargetF-EcrpoD	This study	N/A
pTargetF-EccueR	This study	N/A
pZT100	Li et al., 2014	N/A
pZT-PcopA	This study	N/A
pZT-PcopA$_{-1\ bp}$	This study	N/A
pZT-PcopA$_{+1\ bp}$	This study	N/A
pVS10-RNAP	Belogurov et al., 2007	N/A
pET21a-σ^{70}	This study	N/A
Software and algorithms		
ResMap	Kucukelbir et al., 2014	N/A
UCSF Chimera 1.14	Pettersen et al., 2004	https://www.cgl.ucsf.edu/chimera/

(*Continued on next page*)

Continued

REAGENT or RESOURCE	SOURCE	IDENTIFIER
COOT	Emsley and Cowtan, 2004	https://www2.mrc-lmb.cam.ac.uk/personal/pemsley/coot/
Phenix	Adams et al., 2010	https://www.phenix-online.org/
UCSF ChimeraX 1.0	Goddard et al., 2018	https://www.rbvi.ucsf.edu/chimerax/
PyMol v.2.3.2	Schrödinger	https://pymol.org/2/
Clustal Omega	Sievers and Higgins, 2014	https://www.ebi.ac.uk/Tools/msa/clustalo/
ESPript 3.0	Robert and Gouet, 2014	https://espript.ibcp.fr/ESPript/ESPript/
cryoSPARC v2.15	Punjani et al., 2017	https://cryosparc.com/
RELION 3.1	Zivanov et al., 2020	N/A

RESOURCE AVAILABILITY

Lead contact

Further information and requests for resources and materials should be directed to and will be fulfilled by the Lead Contact, Bin Liu (liu00794@umn.edu).

Material availability

Materials are available upon reasonable request.

Data and code availability

The cryo-EM density maps of our CueR-TAC complex have been deposited in the Electron Microscopy Data Bank under the accession number EMD-22184 (without RNA transcript), EMD-22185 (with RNA transcript) and EMD-22289 (combined map with clearer σNCR density). The corresponding atomic coordinates for the atomic model have been deposited in the Protein Data Bank under the accession number 6XH7 (without RNA transcript) and 6XH8 (with RNA transcript).

EXPERIMENTAL MODEL AND SUBJECT DETAILS

For clone construction, we used the *Escherichia coli* strain DH5α; for recombinant protein expression, we used the *Escherichia coli* strain BL21(DE3); for *in vivo* promoter activity test, we used *Escherichia coli* strains *Ec*-parent, *Ec*-CueR-SETm and *Ec*-σ^{70}-RSKm. Bacteria were grown at 37 °C as described in the Method Details section.

METHOD DETAILS

Purification of RNA polymerase core enzyme and preparation of σ^{70}-RNAP holoenzyme

To express σ^{70} protein, the coding fragment was cloned into pET21a plasmid between *Nhe I* and *Hind III* sites to produce pET21a-σ^{70}. Mutations in σ^{70} were introduced by oligos on pET21a-σ^{70} plasmid following the Quickchange site-directed mutagenesis protocol (Stratagene). All oligonucleotides for constructing clones are listed in Table S2. The procedures for expression and purification of *E. coli* RNAP core enzyme and σ^{70} have followed the reported protocol (Belogurov et al., 2007; Liu et al., 2017; Zuo and Steitz, 2015). *E. coli* core RNAP was expressed in *E. coli* BL21(DE3) and purified using HisTrap HP affinity chromatography column (GE Healthcare), followed by HiTrap Heparin HP column (GE Healthcare), HiTrap Q HP anion exchange chromatography column (GE Healthcare), and HiLoad 16/600 Superdex 200 pg size-exclusion chromatography column. Wild-type and mutant σ^{70} were expressed in *E. coli* BL21(DE3) and purified using HisTrap HP affinity chromatography column (GE Healthcare), followed by HiTrap Heparin HP column (GE Healthcare) and HiLoad 16/600 Superdex 200 pg size-exclusion chromatography column. The σ^{70}-RNAP holoenzyme was assembled by mixing the purified core enzyme with purified σ^{70} protein (1:3 molar ratio) at room temperature for 15 minutes followed by size exclusion chromatography to remove the extra σ^{70} protein (Zuo and Steitz, 2015).

Expression and purification of CueR

For construction of the plasmid pET21a-CueR, the *E. coli* CueR gene was PCR-amplified from *E. coli* genomic DNA and ligated into pET21a vector with C-terminal 6×His-tag using *Nde I* and *Xho I* restriction

sites. Mutations in the plasmid were introduced by oligos following the Quickchange-site-directed mutagenesis protocol (Stratagene).

All constructs were transformed into chemically competent *E. coli* BL21(DE3) cells. The cells were grown in LB medium with 100 μg/mL ampicillin at 37 °C to the OD_{600} value of 0.6, and protein expression was induced with 0.5 mM isopropyl β-d-1-thiogalactopyranoside (IPTG) at 20 °C for 16 h. The harvested cells were suspended in lysis buffer containing 50 mM Tris-HCl, pH 8.0, 300 mM NaCl, 10 mM imidazole, 5% (v/v) glycerol and lysed via sonication. The lysate was then centrifuged at 80,000 g for 1 h. The recombinant CueR protein was purified through a 5-mL HisTrap column (GE Healthcare) and 5-mL HiTrap Heparin column (GE Healthcare) and further loaded onto a gel filtration column, 120-mL HiLoad 16/600 Superdex 200 in a buffer containing 20 mM Tris-HCl, pH 8.0, 150 mM NaCl, 5 mM DTT. The final sample was aliquoted, flash-frozen in liquid nitrogen, and stored at −80 °C until use.

Assembly and purification of *E. coli* CueR-TAC complex

The synthesized promoter DNA used in the assembly includes the region from −10 element and −35 element of the P_{copA} (Figure 1A). The promoter DNA was prepared by annealing non-template (NT) strand DNA to an equal molar amount of template (T) strand DNA (Table S2). The CueR-TAC complexes were assembled by incubating σ^{70}-RNAP holoenzyme, the DNA promoter and CueR protein (1:3:6 molar ratio) in a buffer containing 20 mM Tris-HCl, pH 7.5, 50 mM NaCl, 5 mM $MgCl_2$ and 5 mM DTT at 37 °C for 15 min without or with GTP and ATP (300 μM each). CueR shows high affinity to +1 transition-metal ions, and a majority of the purified CueR protein should already contain bound metal ion, and therefore, extra metal ion is not added in the reaction. CueR, RNAP, and DNA could form a stable CueR-TAC during the complex assembly for cryo-EM study. The reaction mixture was then purified through Superose 6 Increase 10/300 column (GE Healthcare) to remove the extra CueR protein and nucleic acids.

Cryo-EM sample preparation and data acquisition

A drop of 3.5 μL of the purified CueR-TAC at about 1 μM was applied to Quantifoil R2/2 200 mesh Cu grids (EM Sciences) glow-discharged at 15 mA for 60 s. The grid was then blotted for 3 s at 4 °C and 100% humidity and vitrified by plunging into liquid ethane using a Vitrobot Mark IV (FEI).

Cryo-EM data were acquired using a 300-keV Titan Krios microscope (FEI) equipped with a Falcon III direct electron detector. Automated data acquisition was carried out using EPU software (FEI) in counting mode with a pixel size of 0.89 Å and a defocus range from −1.0 to −2.4 μm. Each micrograph contains 30 dose-framed fractions and was recorded with a dose rate of 0.8 e^-/pixel/sec (1 $e^-/Å^2$/sec). Each fraction was exposed for 1 s, resulting in a total exposure time of 30 s and the total dose of 30 $e^-/Å^2$.

Image processing

Cryo-EM data were processed using cryoSPARC v2.15 (Punjani et al., 2017), and the procedure is outlined in Figures S1 and S2. A total of 4,611 (CueR-TAC without RNA) or 4,498 (CueR-TAC with RNA) movies were collected. Beam-induced motion and mechanical drift were corrected with dose-weighting using the Patch motion correction (Rubinstein and Brubaker, 2015). The contrast transfer functions (CTFs) of the summed micrographs were determined using Patch CTF estimation (Rohou and Grigorieff, 2015). Particles were then automatically picked using Blob picker with the parameters: minimum particle diameter (110 Å) and maximum particle diameter (210 Å). In total, 1,421,781 and 1,299,989 particles were picked with a 384 pixels of box size for CueR-TAC without and with RNA, respectively. Junk particles were removed through three rounds of 2-dimensional (2D) classifications. Particles from the good 2D classes were used for *Ab Initio* Reconstruction of four maps. The initial models were low pass filtered to 20 Å and set as the starting references for heterogeneous refinement (3-dimensional [3D] classification) in cryoSPARC v2.15. Particles in good 3D classes were selected to perform homogeneous refinement in cryoSPARC v2.15 and then imported into RELION-3.1 (Zivanov et al., 2020) using csparc2star.py module (Asarnow et al., 2019). To improve the map quality and interpretability of the CueR part in the CueR-TACs, the final particle stacks were subjected to signal subtraction to keep only the CueR dimer and the promoter spacer region, followed by masked 3D classification in RELION-3.1. Particles in the good classes (19,894 and 25,244 for CueR-TAC without and with RNA, respectively) from the masked 3D classification were selected, reverted to the original particles, and subjected to further 3D autorefinements to generate the final 3.9 Å and 4.1 Å maps for CueR-TAC without or with a RNA transcript. Because the two CueR-TAC maps are almost identical in the regions of CueR, promoter upstream DNA, and σNCR, the final particles stacks

from the two data sets were combined (45,138 particles in total) and subjected to masked 3D classification focusing on σNCR and the NTD of the proximal CueR subunit with residual signal subtraction. Particles in the good class (14,935) were selected, reverted to original particles, and subjected to another round of 3D autorefinement that resulted in a 4.1-Å map with clearer density for σNCR and its interacting interface with CueR NTD. This map was used as a cross-reference during model building. Resolutions of all maps were determined by gold-standard Fourier shell correlation (FSC) at 0.143 between the two half-maps. Local resolution variation was estimated from the half-maps by ResMap (Kucukelbir et al., 2014).

Model building and refinement

The initial models were generated by docking the previous structures of the components in the RNAP core (PDB 6B6H) into the individual cryo-EM density maps using Chimera (Pettersen et al., 2004) and COOT (Emsley and Cowtan, 2004). The 3.9 Å and 4.1 Å cryo-EM density maps for CueR-TACs and the 4.1 Å cross-reference map allowed to dock RNAP, σ^{70}, and the CueR dimer in Chimera and build the promoter DNA scaffold and the RNA transcript (5′-GAG-3′) in COOT. The ω subunit is visible at lower contours compared with other components of the complex likely owing to a lower occupancy. The bubble region at the template side of CueR-TAC without RNA and the C-terminal helix of ω subunit of CueR-TAC with RNA were not built owing to poor density. The intact models were then refined using Phenix (Adams et al., 2010). In the real-space refinement, minimization global, local grid search, and adp were performed with the secondary structure, rotamer, and Ramachandran restrains applied throughout the entire refinement. 3DFSC calculation shows the cryo-EM maps have sphericity values of 0.733 and 0.758 for CueR-TAC without and with RNA, respectively, suggesting the maps have sampled majority of the angular space and do not suffer from major directional resolution anisotropy issue (Tan et al., 2017). The split cryo-EM maps were generated using color zone with 1.5 Å coloring radius in volume viewer of Chimera (Pettersen et al., 2004). The final models have good stereochemistry by evaluation in MolProbity (Chen et al., 2010). Map reconstruction quality was also evaluated by Mtriage (Afonine et al., 2018) in Phenix. The statistics of cryo-EM data collection, 3D reconstruction and model refinement were shown in Table S1. All figures were generated using UCSF ChimeraX (version 1.0) (Goddard et al., 2018) and PyMol (Schrödinger, v.2.3.2). Sequence alignments were performed using Clustal Omega (Sievers and Higgins, 2014) and the online server ESPript 3.0 (Robert and Gouet, 2014).

In vitro transcription assay

In vitro transcription assays were performed using linear promoter DNA fragment as template (Shi et al., 2020) with minimal modification. First, 20 nM of 153 bp P_{copA} fragment (ranging from −103 to +50) was incubated with different concentration of CueR protein (ranging from 0 to 240 nM) at 37 °C for 10 min in transcription buffer (20 mM Tris-HCl, pH 7.9, 50 mM NaCl, 5 mM $MgSO_4$, 1 mM DTT, 0.1 mM EDTA, 5% glycerol) plus 1 μM of $AgNO_3$. To exclude the possible effects of some CueR protein without metal ion and ensure that all the purified CueR protein in the assays could be occupied by +1 transition-metal ions, we added 1 μM $AgNO_3$ into the transcription buffer. After that, 100 nM RNAP holoenzyme, which was assembled by mixing 100 nM RNAP core and 300 nM σ^{70}, was added and incubated at 37 °C for another 10 min. Transcription was initiated by the addition of 50 μM CTP, UTP and ATP, 5 μM GTP, and 1 μCi of [α-^{32}P]GTP. The reactions were carried out at 37 °C for 10 min and then stopped by 1 volume of 95% formamide solution. RNA products were heated at 70 °C for 5 min and then analyzed on denaturing (7 M urea) 16% polyacrylamide gel electrophoresis (PAGE).

DNA-binding analysis

The electrophoretic mobility shift assays (EMSA) were performed following a reported protocol (Shi et al., 2020) with slight modification. First, 10 nM of fluorescein-labeled promoter fragments were incubated with different concentrations of CueR protein (ranging from 0 to 480 nM) and then were mixed with 25 nM σ^{70}-RNAP holoenzyme in transcription buffer plus 1 μM of $AgNO_3$ for 10 min at 37 °C. In this assay, we also added 1 μM $AgNO_3$ to ensure that all the purified CueR protein in the assays could be occupied by +1 transition-metal ions. Then, 10 μg/mL of heparin was added and incubated for 5 min at 37 °C. For comparing the promoter binding of σ^{70}-RNAP in the absence or presence of CueR protein, similar procedures were applied except that different concentrations of σ^{70}-RNAP holoenzyme (ranging from 0 to 200 nM) were used. Afterward, samples were loaded on 6% native 0.5×TBE-PAGE. Gels were scanned by Amersham Typhoon scanner (GE Healthcare).

E. coli mutant construction

Mutations in *E. coli* were constructed based on a K12 MG1655 strain with deletion of *lacZ* gene (renamed as *Ec*-parent here) (Hu et al., 2016) using a CRISPR-Cas9 system (Jiang et al., 2015). Briefly, a small guide RNA

(sgRNA) targeting *rpoD* or *cueR* gene was introduced in pTargetF plasmid following the Quickchange-site-directed mutagenesis protocol (Stratagene). The *Ec*-parent strain carrying a Cas9 expressing plasmid pCas was cotransformed with the pTargetF constructs and a donor DNA fragment carrying aimed mutations. Mutants were selected by primer-specific PCR and confirmed by DNA sequencing.

In vivo promoter activity test

In vivo promoter activity was tested using a low-copy *lacZ* reporter fusion plasmid named as pZT100 (Li et al., 2014). A 250-bp P_{copA} fragment was cloned into pZT to produce the pZT-P_{copA} using the ClonExpress II One-Step Cloning Kit (Vazyme). Mutations in pZT-P_{copA} were also introduced by oligos following the Quickchange-site-directed mutagenesis protocol (Stratagene). The pZT constructs were transformed into *E. coli* strains. Bacterial cells were grown to exponential phase in minimal medium and then exposed to 100 μM $CuSO_4$ (Philips et al., 2015) for different time. The levels of β-galactosidase (Hu et al., 2009) were measured to indicate the P_{copA} activities.

QUANTIFICATION AND STATISTICAL ANALYSIS

RNAs from *in vitro* transcription assays and shifted DNAs in EMSA assays were quantified by ImageJ software. Data are shown as mean ± SD from three experiments. The β-galactosidase activity data were obtained from three colonies performed in duplicates for each strain and data are shown as mean ± SEM. Statistical analyses were performed using the unpaired Student's *t*-test (two-tailed) between each of two groups. * $p<0.05$; ** $p<0.01$.